**CCL3 promotes germinal center B cells sampling by follicular regulatory T cells.**

Zachary L. Benet[1], Matangi Marthi[1], Rita Wu[1], Jackson S. Turner[1], Jahan B. Gabayre[1], Michael I. Ivanitskiy[1], Sahil S. Sethi[1], and Irina L. Grigorova[1*].

[1]Department of Microbiology and Immunology, University of Michigan Medical School, 1150 West Medical Center Drive, 5641 Medical Science II, Ann Arbor , Michigan 48109-5620

[*]Please address correspondence to:
Irina L. Grigorova
1150 W. Medical Center Dr
6748 MSII
Ann Arbor, MI 48109
(734) 615-3882 (p)
(734) 764-3562 (f)
igrigor@umich.edu
ORCID: 0000-0002-4963-7403

**ABSTRACT**

Previous studies and our findings suggest upregulated expression of proinflammatory chemokines CCL3/4 in germinal center (GC) centrocytes. However, the role of CCL3/4 for centrocyte interactions with follicular T cells and regulation of humoral immunity is poorly understood. We found that CCL3 promotes chemotaxis of Tfr cells *ex vivo*. *In vivo* CCL3 is not required for Tfr cells recruitment of into the GC light zone. However, B cells-intrinsic production of CCL3 promotes their direct interactions and negative regulation by follicular regulatory T cells (Tfr) within GCs.

## INTRODUCTION

CCL3 and CCL4 (MIP1-$\alpha$ and MIP1-$\beta$) are proinflammatory chemokines that are secreted by various types of immune cells upon activation and play important roles in inflammatory responses and multiple other processes (Menten, Wuyts et al. 2002, Maurer and von Stebut 2004). In B cell cultures with naive, memory, or GC B cells, the cross-linking of B cell receptors (BCRs) upregulates expression and secretion of CCL3/4 (Krzysiek, Lefevre et al. 1999, Bystry, Aluvihare et al. 2001). In addition, analysis of published GC microarray data suggests that expression of CCL3/4 may be elevated in GC centrocytes compared to centroblasts (Caron, Le Gallou et al. 2009, Compagno, Lim et al. 2009, Victora, Dominguez-Sola et al. 2012). Despite multiple indications that CCL3/4 is secreted by activated and GC B cells, the significance of B-cell intrinsic production of proinflammatory chemokines for regulation of humoral response is unclear.

In 2001 Bystry et al. demonstrated that a subset of splenic CD4 T cells that were CD25$^{high}$, expressed high levels of TGF-$\beta$ and CTLA-4, and had a suppressive phenotype *ex vivo,* could migrate to CCL4 (but not CCL3) in transwell assays. The above observations raised the possibility that CCL4 may promote Tregs' interactions with activated B cells or dendritic cells (which also produce CCL3/4) to regulate B cell responses. However, whether more recently identified subset of follicular resident Tregs can respond to CCL3 or CCL4 has been unclear (Lim, Hillsamer et al. 2005, Alexander, Tygrett et al. 2011, Chung, Tanaka et al. 2011, Linterman, Pierson et al. 2011).

65 Tfr cells are a subset of FoxP3$^{pos}$ Tregs that play a role in the control of GC responses.
66 While the majority of Tfr cells arise from natural Tregs, some can be induced from
67 foreign antigen-specific Th cells (Aloulou, Carr et al. 2016). Similarly to Tfh cells, Tfr cells
68 develop in the secondary lymphoid organs following foreign antigen challenge, express
69 the transcription factor Bcl6, upregulate surface expression of CXCR5, PD1 and ICOS
70 receptors, and localize to the follicles and the GCs (Chung, Tanaka et al. 2011,
71 Linterman, Pierson et al. 2011, Wollenberg, Agua-Doce et al. 2011). Deficiency in Tfr
72 cells has been reported to induce a 1.5 to 2-fold increase in GC size at the peak of GC
73 response (Chung, Tanaka et al. 2011, Linterman, Pierson et al. 2011, Wollenberg, Agua-
74 Doce et al. 2011), to affect Tfh cell's cytokine production and Ab class-switching (Sage,
75 Francisco et al. 2013, Sage, Paterson et al. 2014, Wu, Chen et al. 2016), to increase
76 recruitment of non-foreign antigen (Ag)-specific B cell clones into GCs (Linterman,
77 Pierson et al. 2011, Wu, Chen et al. 2016), and to promote development of self-reactive
78 antibodies (Wu, Chen et al. 2016, Botta, Fuller et al. 2017) and even autoimmunity in
79 influenza-infected mice (Fu, Liu et al. 2018). While multiple mechanisms of Tfr cells'
80 action have been suggested based on the *in vivo* and *ex vivo* studies (Alexander, Tygrett
81 et al. 2011, Sage, Francisco et al. 2013, Sage, Paterson et al. 2014, Wing, Ise et al.
82 2014, Wing and Sakaguchi 2014, Sage, Ron-Harel et al. 2016), whether *in vivo* Tfr cells
83 only regulate Tfh cells and thus indirectly control GC responses or can also act on the
84 GC B cells directly remains an open-ended question.
85
86 Here we investigated the role of B cell-intrinsic production of CCL3 in the regulation of
87 GC responses. Based on 2-photon imaging of murine lymph nodes we found that
88 production of CCL3 by foreign Ag-specific GC B cells promotes their sampling and direct
89 inhibition by Tfr at the peak of GC response.
90
91 **RESULTS**
92 **A small subset of GC centrocytes upregulates expression of CCL3 and CCL4.**
93 Based on the previous microarray data (Caron, Le Gallou et al. 2009, Compagno, Lim et
94 al. 2009, Victora, Dominguez-Sola et al. 2012) GC centrocytes (CC) may have elevated
95 expression of CCL3/4 compared to centroblasts (CB). To verify expression of *Ccl3* and
96 *Ccl4* in murine GC B cells, we performed qRT-PCR analysis of GC CC, CB and non-GC

97 B cells sorted from the draining lymph nodes (dLNs) of immunized mice at 10 days post
98 immunization (d.p.i) (**Fig. 1a**). Consistent with previous microarray analysis, we found
99 that expression of CCL3/4 is upregulated in murine GC CC compared to CB (**Fig. 1b, c**).
100
101 **CCL3 and CCL4 induce chemotaxis of follicular regulatory T cells *ex vivo.***
102 To determine whether CCL3/4 may promote chemotaxis of follicular T cells *ex vivo* we
103 performed transwell migration analysis of CD4 T cells isolated from dLNs of mice at 10
104 d.p.i. with OVA in Ribi adjuvant. CXCR5$^{high}$ PD1$^{high}$ FoxP3$^{+}$ Tfr cells transmigrated in
105 response to CCL3 chemokine (**Fig. 2a, b**). Similar trends were observed for CXCR5$^{low}$
106 PD1$^{low}$ FoxP3$^{+}$ and CXCR5$^{int}$ PD1$^{int}$ FoxP3$^{+}$ CD4 T cells (**Fig. 2a, b**). We also observed
107 transmigration of Tfr and other regulatory T cell subsets to CCL4 (**Fig. 2c**). The observed
108 transmigration was predominantly due to chemotaxis rather than chemokinesis, since
109 addition of CCL3 or CCL4 chemokines to both the upper and the lower wells of the
110 transwell chamber did not promote Tregs' transmigration (**Fig. 2b, c**). No significant
111 transmigration of Tfh cells (CXCR5$^{high}$ PD1$^{high}$ FoxP3$^{-}$) to CCL3 and CCL4 chemokines
112 was observed (**Fig. 2d, e**). These data suggest that CCL3 and CCL4 can induce
113 chemotaxis of Tfr and possibly other Treg cells *ex vivo*.
114
115
116
117 **CCL3 does not recruit Tfr cells into the GC light zone.**
118 To determine if CCL3/4 play a role in the regulation of GC size, we utilized CCL3-KO
119 mice (Cook, Beck et al. 1995). In unimmunized CCL3-KO and WT mice we observed no
120 significant difference in the GC B cells numbers in peripheral lymph nodes (pLNs),
121 spleens, mesenteric LNs (mLNs) and peyer patches (PP) (**Fig. 3a**). However, at 10 d.p.i.
122 we detected a small, but significant increase in the GC response in the dLNs of CCL3-
123 KO mice compared to WT that was independent of the antigen or the adjuvant used
124 (**Fig. 3b-e**). We then tested whether in littermate-control CCL3$^{-/-}$ mice GCs were also
125 elevated compared to CCL3$^{+/+}$, and confirmed the observed phenotype (**Fig. 3f, g)**.
126 Interestingly, treatment of WT or CCL3-KO mice with CCL4-neutralizing antibodies
127 during formation of GCs, at 7 d.p.i., did not lead to further increase in the GC response
128 (**Supplementary Fig. 1**). The observed accumulation of GC B cells at 10 d.p.i. was not
129 due to significant changes in formation of Tfh and Tfr cells or in their ratio (**Fig. 3h-j**). In

130 addition, the increase in GC B cells did not lead to significant rise in the numbers of
131 plasmablasts (PB) at 10 d.p.i. (**Fig. 3k, l**).
132
133 Our observations that CCL3 promotes Tfr cells chemotaxis *ex vivo* and plays a role in
134 the control over GC size *in vivo* led us to ask whether CCL3 produced by GC centrocytes
135 recruits Tfr cells from the follicles into the GCs. If this hypothesis is correct, the
136 frequency of Tfr cells in the GC light zone should be reduced in CCL3-KO mice
137 compared to WT mice. To test this, we analyzed the density of Tregs in the GCs (both in
138 the light and the dark zones) and in the follicles of the draining LNs from immunized
139 CCL3–KO and WT mice. Fixed LNs were sectioned and stained with fluorescently
140 conjugated antibodies towards IgD, CD35, CD4, and FoxP3 and analyzed by confocal
141 microscopy (**Figure 4a-c**). In WT mice, $CD4^+$ $FoxP3^+$ Treg cells were enriched in the
142 follicles compared to the GCs (**Figure 4c, d**). In contrast to the expected decrease in the
143 Tfr cell frequency within the GC light zone of CCL3-KO mice, the density and recruitment
144 index of $CD4^+$ $FoxP3^+$ cells in the light zones of CCL3 KO and WT mice were
145 comparable (**Figure 4d, e**). However, the recruitment index calculated for Tregs' access
146 into the GC dark zone relative to the follicle was higher for CCL3-KO mice (**Figure 4e**).
147 Interestingly, we also observed modest enrichment of Tfh cells in the dark zones of GCs
148 in CCL3-KO mice (**Figure 4f, e**). Based on this data we conclude that CCL3/4 is not
149 required for Tfr cells' recruitment into the GC light zone from the follicles, but may play a
150 role in limiting access of follicular T cells to the GC dark zone.
151
152 **Adoptively transferred Tregs can become Tfrs' and be visualized by 2P**
153 **microscopy.** We then asked whether CCL3 could promote individual interactions of Tfr
154 cells with GC B cells *in vivo*. To directly test this, we developed an imaging strategy that
155 enabled visualization of adoptively transferred Tregs within the GC-containing follicles of
156 living mice using 2-photon (2P) microscopy (**Fig. 5a**). Because intravenous injection of
157 Tregs is insufficient to get enough of the transferred Tregs into peripheral LNs for
158 microscopy analysis, we utilized the fact that adoptively transferred Tregs undergo
159 proliferation in recipient $FoxP3^{DTR}$ mice upon diphtheria toxin (DTx)-induced ablation of
160 DTx receptor (DTR)-expressing resident Tregs (Kim, Rasmussen et al. 2007). Of note,
161 while treatment of $FoxP3^{DTR}$ mice with DTx leads to development of severe autoimmune
162 disease, pre-transfer of $10^6$ polyclonal Tregs rescues $FoxP3^{DTR}$ mice from autoimmunity

163 (Kim, Rasmussen et al. 2007). To generate mice with a high number of brightly
164 fluorescent Tfr cells, we first transferred $10^6$ polyclonal Tregs that expressed both Foxp3-
165 GFP and tdTomato into $Foxp3^{DTR}$ mice (Bettelli, Carrier et al. 2006, Kim, Rasmussen et
166 al. 2007). We then treated the $Foxp3^{DTR}$ recipients with 5 μg of DTx two times, one week
167 apart. As reported before, following transient ablation of $Foxp3^{DTR}$ Tregs, the adoptively
168 transferred Tregs as well as the remaining endogenous Tregs underwent vigorous
169 proliferation. At 14 days following the initial DTx treatment, tdTomato Tregs represented
170 about 50% of all Tregs in the blood (**Fig. 5b**). We then co-transferred Duck Egg
171 Lysozyme (DEL)-specific HyHEL10 B cells expressing CFP, OVA-specific OTII CD4 T
172 cells expressing GFP, as well as non fluorescent HyHEL10 B and OTII T cells into the
173 same recipient mice and induced their recruitment into the GCs by s.c. immunization
174 with DEL-OVA as previously described (Allen, Okada et al. 2007). By 8 d.p.i. the overall
175 levels of Tregs in the blood had returned to normal (**Fig. 5b**). Based on confocal and flow
176 cytometry analysis we determined that over a fifth of $CD4^+Foxp3^+$ cells from dLNs
177 expressed tdTomato and that $tdTomato^+$ cells were almost exclusively $Foxp3^+$ (**Fig. 5c,**
178 **d**). Additionally, $tdTomato^+$ $Foxp3^+$ cells that were also $CXCR5^{high}$ $PD1^{high}$ had increased
179 expression of $Bcl6^+$ as expected for Tfr cells (**Fig. 5c**). At 7-8 d.p.i. a relatively minor
180 fraction of GC-proximal Tfr cells entered into the GCs, while majority of the cells moved
181 around GCs in proximity to the outer edge GC B cells (**Fig. 5e, Supplementary Movie**
182 **1**). These data suggest that the adoptive transfer of fluorescent Tregs followed by
183 transient ablation of non-fluorescent endogenous Tregs and immunization is sufficient to
184 visualize Tfr cells within GC-associated follicles in living mice by 2P microscopy.
185
186 **GC B cells' CCL3 promotes their contacts with Tfr, but not Tfh cells *in vivo*.**
187 To determine whether GC B cells' intrinsic production of CCL3 promotes their direct
188 interactions with Tfr cells or with Tfh cells *in vivo* we utilized the experimental setup
189 developed by us (**Fig. 5**) and in previous work (Allen, Okada et al. 2007) and outlined in
190 **Figures 6a** and **b**. For analysis of T cell interactions with $CCL3^{+/+}$ and $CCL3^{-/-}$ GC B
191 cells, recipient mice were co-transferred with $CCL3^{+/+}$ HyHEL10 B cells that expressed
192 CFP and $CCL3^{-/-}$ HyHEL10 B cells that expressed GFP. To determine Tfr cells'
193 interactions with GC B cells we tracked $tdTomato^+$ Tfr cells when they contacted or
194 passed through the GCs, and analyzed their interactions with fluorescent $CCL3^{+/+}$ and
195 $CCL3^{-/-}$ foreign Ag-specific HyHEL10 B cells within the same GCs (**Fig. 6c,**

196 **Supplementary Movie 2**). To take into account the ambiguity of correct identification of
197 B-T cell interactions by 2P imaging, we used both "strict" and "non-strict" definitions of
198 contacts between GC B cells and follicular T cells. By "strict" we define the interactions
199 that based on the cell colocalization analysis in 3D have taken place with high
200 confidence. By "non-strict" interactions we identify all likely interactions identified based
201 on cell proximity, including the "strict" interactions. The data was analyzed in a blinded
202 fashion to avoid possible bias in cell contact definition (**Fig. 6d, Supplementary Movie**
203 **3**). We calculated the normalized contact frequency (NCF) of Tfr cells with fluorescent
204 $CCL3^{+/+}$ and $CCL3^{-/-}$ GC B cells by dividing the total number of Tfr cell contacts with
205 $CCL3^{+/+}$ or $CCL3^{-/-}$ GC B cells by the average numbers of fluorescent B cells of each type
206 present in the imaged GCs. Tfr cells' NCF was lower for $CCL3^{-/-}$ compared to $CCL3^{+/+}$
207 GC B cells in 5 experiments, independently of the "strict" vs "non-strict" B-Tfr cell contact
208 definition (**Fig. 6e-h**). The differences in Tfr cell contact frequencies with $CCL3^{+/+}$ and
209 $CCL3^{-/-}$ GC B cells were not due to distinct migratory properties of $CCL3^{+/+}$ and $CCL3^{-/-}$ B
210 cells (**Supplementary Fig. 6**). In contrast to Tfr cells, OTII Tfh cell NCF with $CCL3^{+/+}$ vs.
211 $CCL3^{-/-}$ GC B was comparable (**Fig. 6e-h, Supplementary Movie 4**). The ratio of T
212 cells' NCF with $CCL3^{+/+}$ vs. $CCL3^{-/-}$ GC B cells was significantly lower for Tfh compared
213 to Tfr cells (**Fig. 6f, h)**.
214
215 While Tfr cells formed more frequent contacts with $CCL3^{+/+}$ GC B cells, duration of Tfr
216 cell interactions with $CCL3^{+/+}$ and $CCL3^{-/-}$ GC B cells was comparable (**Fig. 6i, j**).
217 Additionally, no significant difference in the duration of Tfh cell contacts with $CCL3^{+/+}$ vs.
218 $CCL3^{-/-}$ GC B cells was observed (**Fig. 6i, j**). The vast majority of Tfr and Tfh cell
219 contacts with GC B cells were shorter than 5 min (**Fig. 6i-l**). However, while a substantial
220 number of both Tfh and Tfr cells also formed more prolonged interactions with GC B
221 cells, no Tfr cells' interactions with GC B cells exceeding 7.5 min were observed (**Fig.**
222 **6k, l, Supplementary Movies 3, 4**).
223
224 **Transient depletion of Tregs leads to relative increase in $CCL3^{+/+}$ vs. $CCL3^{-/-}$**
225 **HyHEL10 GC B cells at the peak of GC response.** To determine whether Tfr cells may
226 act on CCL3-proficient GC B cells and modulate their participation in GC response we
227 sought to determine whether transient depletion of Tregs after formation of GCs could

228 affect relative involvement of CCL3 proficient and deficient B cells in the GC response. In
229 order to test that, we co-transferred CCL3$^{+/+}$ and CCL3$^{-/-}$ HyHEL10 B cells into recipient
230 FoxP3$^{DTR}$ mice, immunized mice to promote HyHEL10 cell entry into GC response and
231 then treated mice with diphtheria toxin (DTx) to promote transient depletion of FoxP3$^{+}$
232 cells or with PBS for control (**Fig. 7a**). We hypothesized that CCL3 secreted by GC B
233 cells promotes their direct interactions with and inhibition by Tfr cells. In that case,
234 depletion of Tfr cells should lead to increased expansion of CCL3-proficient compared to
235 CCL3-deficient GC B cells (**Fig. 7b**). As expected, treatment of the recipient mice with
236 DTx at 6 d.p.i. led to significant drop in Tfr cells numbers in 3 days (**Fig. 7c, d**) and small
237 increase in the GC B cell numbers (**Fig. 7e**). Consistent with that, upon the transient Tfr
238 cell depletion, we detected a small increase in CCL3$^{+/+}$ HyHEL10 B cell numbers,
239 however CCL3$^{-/-}$ HyHEL10 GC B cells were virtually unchanged (**Fig. 7f**). As a result of
240 this, there was significant enrichment of CCL3$^{+/+}$ vs. CCL3$^{-/-}$ HyHEL10 B cells within GCs
241 (**Fig. 7g**). Therefore, the data is consistent with direct CCL3-dependent inhibition of GC
242 B cells by Tregs at the peak of GC response (**Fig. 7b**).
243
244
245 **DISCUSSION:**
246 While Tfr cells have been shown to control the numbers, specificity to foreign antigen
247 and cytokine production of Tfh cells that support GC responses *in vivo* (Sage, Francisco
248 et al. 2013, Sage, Paterson et al. 2014, Wing, Ise et al. 2014, Wu, Chen et al. 2016)
249 whether Tfr cells can directly affect GC B cells *in vivo* has not been definitively
250 demonstrated. While this study does not exclude the role of Tfr cells in the regulation of
251 Tfh cell numbers and the magnitude of foreign-Ag specific response, it suggests that
252 secretion of CCL3/4 by B cells is important for direct Tfr-mediated regulation of GC B
253 cells. First, we determined that GC centrocytes upregulate expression of CCL3/4
254 compared to centroblasts. We then showed that Tfr cells as well as the other Treg
255 subsets are responsive to CCL3 and CCL4 in transwell assays and demonstrated that
256 CCL3 production by foreign Ag-specific GC B cells increases their sampling efficiency by
257 Tfr cells. Finally, consistent with a model of direct inhibition of CCL3-producing GC B
258 cells by Tfrs, we found that depletion of regulatory T cells at the peak of the GC
259 response results in a small but significant increase in the numbers of CCL3-proficient,
260 but not CCL3-deficient HyHEL10 GC B cells. Future studies should assess which

261 molecular players, including TGF-β, PD1, CTLA-4, GLUT1, and IL21 (Alexander, Tygrett
262 et al. 2011, Sage, Francisco et al. 2013, Sage, Paterson et al. 2014, Wing, Ise et al.
263 2014, Sage, Ron-Harel et al. 2016, Wu, Chen et al. 2016) may be involved into the
264 observed direct regulation.
265
266 Future studies should examine the impact of B cell-intrinsic CCL3 deficiency on the
267 kinetics of B cell participation in the GC and memory response, and foreign Ag-specific
268 Ab responses and dissect the contribution of Tfr cells to the regulation. They should also
269 assess whether CCL3 contributes to better control over bystander or self-reactive B cell
270 clones in GCs and conveys better protection against development of autoimmunity.
271 Interestingly, although CCL3 and CCL4 are coexpressed in activated and GC B cells,
272 neutralization of CCL4 at the time of GC formation did not promote significant increase in
273 the GC response in WT or CCL3-KO mice. It is possible that CCL4 expression in CCL3
274 KO cells is reduced as has been reported before (Patterson, Pesenacker et al. 2016).
275 Alternatively, CCL4 concentration produced by GC B cells is suboptimal for promotion of
276 Tfr cell response.
277
278 We suggest two possible models that could explain the increased sampling of CCL3-
279 proficient GC B cells by Tfr cells. First, the observed effect could be due to local
280 chemoattraction of Tfr cells to CCL3-secreting GC B cells. Since BCR crosslinking has
281 been reported to induce upregulation of CCL3/4 production in GC B cells (Krzysiek,
282 Lefevre et al. 1999), we hypothesize that GC centrocytes that recently acquired antigen
283 from FDCs (and possibly T cell help) are likely to produce more CCL3/4 than other GC B
284 cells, and thus could form local short-range gradients of these chemokines. In that case,
285 to preserve local CCL3 gradient around migrating GC B cell, secreted CCL3 would have
286 to be rapidly internalized and removed by other cells within GCs. Alternatively to the first
287 model, CCL3 chemokine secreted by GC B cells could be transiently immobilized on the
288 surface of selected GC B cells in association with chemokine-binding
289 glycosaminoglycans (Liang, Triandafillou et al. 2016) and may serve to stabilize very
290 transient probing interactions of GC B cells with Tfr cells that are beyond the resolution
291 capabilities of intravital 2P microscopy. Both of these models can lead to decreased
292 efficiency in productive sampling of CCL3 KO B cells by Tfr cells. Future studies should
293 examine whether CCL3 is uniformly upregulated in GC CC or whether there is a subset

294 of cells with elevated expression of CCL3/4. In the later case the advantage that CCL3$^{hi}$
295 GC B cells may have in contacting Tfr cells may be significantly underestimated.

296 Future studies should address whether CCR5, CCR1, or both of these receptors are
297 involved in the observed CCL3-mediated regulation and interactions between GC B cells
298 and Tfr cells.
299
300 Previous intravital imaging studies of Tfh cell interactions with cognate GC B cells
301 revealed that majority of these encounters are transient (Allen, Okada et al. 2007).They
302 also suggested that a small fraction of the interactions that are more prolonged (> 5-10
303 min) may be more efficient for productive communication between the cells and for GC B
304 cell selection (Qi, Cannons et al. 2008, Shulman, Gitlin et al. 2014). In this study we
305 found that similarly to Tfh cells, a majority of interactions between foreign-antigen
306 specific GC B cells and natural Tfr cells *in vivo* are shorter than 5 min. Interestingly, Tfr
307 cells also formed a few interactions with GC B cells that were more prolonged. However,
308 while a few Tfh cell contacts with GC B exceeded 7.5 min, none of these have been
309 observed for Tfr cells. This discrepancy may be due to non-cognate interactions or very
310 weak cognate interactions between foreign antigen specific GC B cells and natural Tfr
311 cells. Future studies should directly address whether Tfr cells recognize MHCII/self-
312 peptides on GC B cells via T cell receptors (TCR), and how prevalent these cognate
313 interactions are. In addition, whether cognate interactions of Tfr cells with self antigen-
314 presenting GC B cells exert much stronger negative control of potentially self-reactive
315 GC B cells must be examined, as well as the contribution of CCL3 to that regulation.
316
317 In summary, our findings suggest that local CCL3 chemokine production by GC B cells
318 promotes their interactions and direct inhibition by Tfr cells at the peak of GC response.
319
320
321
322
323 **MATERIALS AND METHODES**
324 **Mice, immunizations, and bone marrow chimeras**. C57BL/6 (B6, WT) mice were
325 purchased from the National Cancer Institute, Charles River or Jackson Laboratories.

326 B6-CD45.1 (002014), CCL3-KO (002687), β-actin-CFP (004218), UBC-GFP (004353),
327 Stop-tdTomato (007909) and E2a-Cre (003724) mice were from Jackson Laboratories.
328 HyHEL10 (Allen, Okada et al. 2007), MD4 (Goodnow, Crosbie et al. 1988), OTII
329 (Barnden, Allison et al. 1998), $Foxp3^{EGFP}$, and $Foxp3^{DTR}$ mice were from internal
330 colonies. All mice were housed in specific-pathogen free conditions. Relevant mice were
331 interbred to obtain HyHEL10 $CFP^+$, HyHEL10 $GFP^+$ CCL3-KO, OTII $GFP^+$, OTII
332 $tdTomato^+$, MD4 $CFP^+$, and $tdTomato^+$ $Foxp3^{EGFP}$ mice. 6-12 weeks old mice were
333 immunized s.c. with the protein antigens OVA (Sigma), DEL-OVA (produced as
334 previously described (Allen, Okada et al. 2007)), or NP-KLH (Biosearch Technologies),
335 mixed in either Ribi (Sigma) or Complete Freund Adjuvant (CFA, Sigma). In some
336 experiments 50 μg of anti-CCL4 (R&D clone 46907) or isotype control rat Abs (R&D
337 clone 54447) were s.c. administered into the preimmunized mice. All experiments were
338 performed in compliance with federal laws and institutional guidelines as approved by
339 the University Committee on Use and Care of Animals.
340
341 **Cell isolation, flow cytometry analysis and cell sorting.** Lymphocytes were isolated
342 by homogenizing lymph nodes (LNs) and/or spleens into a single cell suspension in
343 DMEM medium (Corning) containing 2% fetal bovine serum (FBS, Atlanta Biologicals),
344 antibiotics (50 IU/mL of penicillin and 50 *μ*g/mL of streptomycin; Gibco) and 10 mM
345 HEPES (Gibco) and straining through a 70 *μ*m mesh filter (Falcon) in the presence of 20
346 *μ*g/ml of DNase I (Sigma-Aldrich). Red blood cells were lysed using Tris-buffered $NH_4Cl$.
347 The following antibodies and reagents were used for flow cytometry analysis: CD3 (BD,
348 145-2C11), CD4 (BD, RM4-5), CD8 (BD, 53-6.7), CD25 (BD, PC61.5), B220 (BD, RA3-
349 6B2), CD19 (BD, 1D3), CXCR5 (BD, 2G8), Fas (BD, Jo2), IgM (BD, R6-60.2), $IgM^a$ (BD,
350 DS-1), Vβ5 (BD, MR9-4), CD43 (BD, S7), CD19 (Biolegend, 6D5), CD45.1 (Biolegend,
351 A20), CD45.2 (Biolegend, 104), IgD (Biolegend, 11-26c.2a), PD-1 (Biolegend, RMP1-
352 30), CXCR4 (eBiosciences, 2B11), CD86 (Biolegend, GL1), Foxp3 (eBiosciences, FJK-
353 16s), GL-7 (eBiosciences, GL-7), SA-qDot607 (Life Technologies), SA-DyLight 488
354 (Biolegend). Single-cell suspensions were incubated with biotinylated antibodies for 20
355 minutes on ice, washed twice with 200 μl PBS supplemented with 2% FBS, 1 mM EDTA,
356 and 0.1% NaN (FACS buffer), and then incubated with fluorophore-conjugated
357 antibodies and streptavidin for 20 minutes on ice, and washed twice more with 200 μl

358 FACS buffer. For FoxP3 staining the cells were permeabilized and stained using FoxP3
359 staining buffer set (eBioscience) according to the manufacturer's instructions. Cells were
360 then resuspended in FACS buffer for acquisition. All flow cytometry analyses and cell-
361 sorting procedures were done using FACSCanto II and FACSAria IIIu respectively.
362 FlowJo Software (v 9.7; TreeStar) was used for data analyses and plot rendering.
363
364 **Cell purification and adoptive transfers**. For adoptive transfers, cells were isolated
365 from combined spleens and LNs of donor mice and CD4 T cells or B cells were enriched
366 using autoMACS (Miltenyi Biotec) as described before (Allen, Okada et al. 2007). The
367 purity of B cells was >95%, and CD4 T cells >70% for all experiments. Lymphocytes
368 were adoptively transferred by intravenous injection into the lateral tail vein.
369
370 **Generation of mice with Tregs and Tfr cells expressing tdTomato.** In order to
371 generate mice with fluorescent Tregs the following scheme was utilized: first, tdTomato
372 expressing mice were crossed with Foxp3$^{EGFP}$ mice. Second, tdTomato$^{+}$Foxp3$^{EGFP}$ Tregs
373 were sorted and adoptively transferred into Foxp3$^{DTR}$ mice where endogenous Tregs
374 were transiently ablated by DTx treatment (Sigma). To sort tdTomato expressing Tregs,
375 the LNs and spleens from the tdTomato$^{+}$Foxp3$^{EGFP}$ mice were combined and lymphocyte
376 suspension was prepared as described above. The lymphocytes were separated from
377 RBCs using Ficoll-Paque (GE Healthcare) gradients per manufacturer's instructions
378 using 14 mL round bottom tubes (Falcon). Single cell suspensions were enriched for
379 CD4$^{+}$ T cells as described above. Following the enrichment, EGFP$^{+}$ cells were sorted
380 into DMEM medium supplemented with 10% FCS. The purity of sorted Tregs as
381 determined by intracellular Foxp3 staining was > 99%. About 0.8-1.5 million of purified
382 tdTomato$^{+}$ Tregs were then transferred into recipient Foxp3$^{DTR}$ mice via tail vein injection.
383 Finally, one day later the endogenous nonfluorescent Tregs in the recipient Foxp3$^{DTR}$
384 mice were ablated by intraperitoneal injection of 5 $\mu$g/kg of DTx in PBS. The DTx
385 treatment was repeated once more a week later.
386
387 **Cell culture and chemotaxis.** Transwells with 5 $\mu$m pore size (Corning) were used.
388 CD4 T cells were isolated and enriched as described above from draining peripheral LNs
389 of mice s.c. immunized with OVA in Ribi at 10 days following immunization. T cells were
390 resuspended with RPMI 1640 (Corning) supplemented with 2% fatty acid free BSA

391 (Sigma-Aldrich), 10 mM HEPES, 50 IU/mL of penicillin, and 50 mg/mL of streptomycin
392 (HyClone). For chemotaxis analysis the lower chambers of transwells were filled with the
393 same medium mixed with various concentrations of CCL3 or CCL4 chemokines
394 (PeproTech). For chemokinesis analysis both upper and lower chambers of transwells
395 were filled with either 200 ng/mL of CCL3 or with 400 ng/mL CCL4. Transwells with
396 chemokines and resuspended CD4 T cells were incubated at 37ºC and 5% $CO_2$ for 10
397 minutes. After that, CD4 T cells were placed in the upper chambers of transwells at
398 $4x10^5$ cells per well and incubated at 37ºC and 5% $CO_2$ for 3 hours. Two to three
399 replicas per condition have been performed per experiment. The transmigrated fraction
400 of cells was stained and analyzed via flow cytometry. Chemotactic index was calculated
401 as the ratio of cells that transmigrated to chemokine compared to no cytokine control.
402
403 **Two Photon Microscopy.** Inguinal LNs (ILNs) were either explanted or surgically
404 exposed for intravital imaging and perfused as previously described (Allen, Okada et al.
405 2007, Grigorova, Schwab et al. 2009). ILNs were imaged with a Leica SP5 II (Leica
406 Microsystems) fitted with a MaiTai Ti:Sapphire laser (Sepctra-Physics) that was tuned to
407 870 nm. Each *xy* plane spanned 435 $\mu$m x 435 $\mu$m and with z spacing ranging from 2-3
408 $\mu$m detecting emission wavelengths of 430-450 nm (second harmonic emission of
409 collagen), 465-500 nm (for $CFP^+$ cells), 520-550 nm (for $GFP^+$ cells), and >560 nm (for
410 $tdTomato^+$ cells), every 20-25 seconds. Images were acquired by Leica Advanced
411 Fluorescent Suite (Leica Microsystems). Analysis of the imaging data and generation of
412 3D rotations and time-lapse image sequences were performed using Imaris 7.6.5 x 64
413 (Bitplane). Videos were processed with a median noise filter. Semi-automated cell
414 tracking in 3D was performed with Imaris 7.6.5 x 64, and then verified and corrected
415 manually. 3-dimensional GC volume was defined based on the distribution of HyHEL10
416 CFP B cells by combination of visual analysis and a custom-made MATLAB program
417 that performed time integrated image rendering of CFP signal. $TdTomato^+$ Tregs and Th
418 that transited within the follicles and GCs were tracked. Their interaction with WT and
419 CCL3-KO B cells within defined GCs volume were visually identified and categorized
420 either as a strict contact as defined when cell-to-cell contact was unambiguous or a non-
421 strict contacts where cells could be observed in extreme proximity (~1 $\mu$m). Finally, we
422 normalized the number of contacts to the average number of WT or CCL3-KO B cells
423 within the GC volume accessible to Tfr or Tfh cells to arrive at a normalized contact

frequency. Annotation and final compilation of videos was performed in Adobe After Effects CS5.5 (Adobe).

**RT-PCR Analysis**. RNA from sorted cells was obtained using RNeasy Kit (Qiagen) following the manufacturer's instructions. RNA was treated with DNase to remove genomic DNA (Ambion). The concentration of RNA was calculated using a NanoDrop 2000 (Thermo) and cDNA was synthesized using a SuperScript III kit (Invitrogen) following the manufacturer's instructions. Preamplification of target genes was performed using PreAmp Kit (AB Biosystems) for 10 cycles. TaqMan assays were obtained from Applied Biosystems and RT-PCR was carried out on a RealPlex 2 (Eppendorf). Expression levels of CCL3/4 were normalized to the level of β2m.

**Statistical analysis.** All statistical tests were computed with PRISM (GraphPad) after consultation with a University of Michigan Center for Statistical Consultation and Research representative. Statistical analysis of data normalized to the control samples were performed using a one-sample *t*-test. For comparisons between two groups *t*-test was utilized. Welch's correction was applied for data with unequal variances. For data in which more than two groups or more than two time points were analyzed, two-way ANOVA followed by Dunnet post-hoc analysis was done. In cases where we did not assume normally distributed data and the data was from paired measurements, we used the Wilcoxon signed-rank test. *P* values of less than 0.05 were considered statistically significant. All statistically significant results were labeled. No samples were excluded from the analysis.

## AUTHOR CONTRIBUTIONS

Z.L.B. planned, performed and analyzed experiments and prepared the manuscript; M.M., R.W. and J.S.T. helped with various aspects of other experiments; J.B.G., M.I.I., and S.S.S. performed blind analysis of the imaging data; I.G. planned, performed and analyzed experiments, and prepared the manuscript.

## ACKNOWLEDGMENTS

We thank W. Dunnick and E. Perkey for discussions; J. Cyster (University of California San Francisco), W. Zhou (University of Michigan Medical school), and A. Rudensky (Memorial Sloan Kettering Cancer Center) for provision of mice; the University of Michigan flow cytometry core for cell sorting assistance. Supported by the American Heart Association (14PRE19960005) to Z.B., by the Herman and Dorothy Miller Award for Innovative Immunology Research to J.S.T. and Z.L.B., and National Institute of Health (R01 AI106806) to I.G. The authors declare no competing financial interests.

**REFERENCES**

489 Alexander, C. M., L. T. Tygrett, A. W. Boyden, K. L. Wolniak, K. L. Legge and T. J.
490 Waldschmidt (2011). "T regulatory cells participate in the control of germinal centre
491 reactions." Immunology **133**(4): 452-468.
492 Allen, C. D., T. Okada, H. L. Tang and J. G. Cyster (2007). "Imaging of germinal center
493 selection events during affinity maturation." Science **315**(5811): 528-531.
494 Aloulou, M., E. J. Carr, M. Gador, A. Bignon, R. S. Liblau, N. Fazilleau and M. A.
495 Linterman (2016). "Follicular regulatory T cells can be specific for the immunizing
496 antigen and derive from naive T cells." Nat Commun **7**: 10579.
497 Barnden, M. J., J. Allison, W. R. Heath and F. R. Carbone (1998). "Defective TCR
498 expression in transgenic mice constructed using cDNA-based alpha- and beta-chain
499 genes under the control of heterologous regulatory elements." Immunol Cell Biol **76**(1):
500 34-40.
501 Bettelli, E., Y. Carrier, W. Gao, T. Korn, T. B. Strom, M. Oukka, H. L. Weiner and V. K.
502 Kuchroo (2006). "Reciprocal developmental pathways for the generation of pathogenic
503 effector TH17 and regulatory T cells." Nature **441**(7090): 235-238.
504 Botta, D., M. J. Fuller, T. T. Marquez-Lago, H. Bachus, J. E. Bradley, A. S. Weinmann,
505 A. J. Zajac, T. D. Randall, F. E. Lund, B. Leon and A. Ballesteros-Tato (2017). "Dynamic
506 regulation of T follicular regulatory cell responses by interleukin 2 during influenza
507 infection." Nat Immunol **18**(11): 1249-1260.
508 Bystry, R. S., V. Aluvihare, K. A. Welch, M. Kallikourdis and A. G. Betz (2001). "B cells
509 and professional APCs recruit regulatory T cells via CCL4." Nat Immunol **2**(12): 1126-
510 1132.
511 Caron, G., S. Le Gallou, T. Lamy, K. Tarte and T. Fest (2009). "CXCR4 expression
512 functionally discriminates centroblasts versus centrocytes within human germinal center
513 B cells." J Immunol **182**(12): 7595-7602.
514 Chung, Y., S. Tanaka, F. Chu, R. I. Nurieva, G. J. Martinez, S. Rawal, Y. H. Wang, H.
515 Lim, J. M. Reynolds, X. H. Zhou, H. M. Fan, Z. M. Liu, S. S. Neelapu and C. Dong
516 (2011). "Follicular regulatory T cells expressing Foxp3 and Bcl-6 suppress germinal
517 center reactions." Nat Med **17**(8): 983-988.
518 Compagno, M., W. K. Lim, A. Grunn, S. V. Nandula, M. Brahmachary, Q. Shen, F.
519 Bertoni, M. Ponzoni, M. Scandurra, A. Califano, G. Bhagat, A. Chadburn, R. Dalla-
520 Favera and L. Pasqualucci (2009). "Mutations of multiple genes cause deregulation of
521 NF-kappaB in diffuse large B-cell lymphoma." Nature **459**(7247): 717-721.
522 Cook, D. N., M. A. Beck, T. M. Coffman, S. L. Kirby, J. F. Sheridan, I. B. Pragnell and O.
523 Smithies (1995). "Requirement of MIP-1 alpha for an inflammatory response to viral
524 infection." Science **269**(5230): 1583-1585.
525 Fu, W., X. Liu, X. Lin, H. Feng, L. Sun, S. Li, H. Chen, H. Tang, L. Lu, W. Jin and C.
526 Dong (2018). "Deficiency in T follicular regulatory cells promotes autoimmunity." J Exp
527 Med **215**(3): 815-825.
528 Goodnow, C. C., J. Crosbie, S. Adelstein, T. B. Lavoie, S. J. Smith-Gill, R. A. Brink, H.
529 Pritchard-Briscoe, J. S. Wotherspoon, R. H. Loblay, K. Raphael and et al. (1988).
530 "Altered immunoglobulin expression and functional silencing of self-reactive B
531 lymphocytes in transgenic mice." Nature **334**(6184): 676-682.
532 Grigorova, I. L., S. R. Schwab, T. G. Phan, T. H. Pham, T. Okada and J. G. Cyster
533 (2009). "Cortical sinus probing, S1P1-dependent entry and flow-based capture of
534 egressing T cells." Nat Immunol **10**(1): 58-65.
535 Kim, J. M., J. P. Rasmussen and A. Y. Rudensky (2007). "Regulatory T cells prevent
536 catastrophic autoimmunity throughout the lifespan of mice." Nat Immunol **8**(2): 191-197.
537 Krzysiek, R., E. A. Lefevre, W. Zou, A. Foussat, J. Bernard, A. Portier, P. Galanaud and
538 Y. Richard (1999). "Antigen receptor engagement selectively induces macrophage

539 inflammatory protein-1 alpha (MIP-1 alpha) and MIP-1 beta chemokine production in
540 human B cells." J Immunol **162**(8): 4455-4463.
541 Liang, W. G., C. G. Triandafillou, T. Y. Huang, M. M. Zulueta, S. Banerjee, A. R. Dinner,
542 S. C. Hung and W. J. Tang (2016). "Structural basis for oligomerization and
543 glycosaminoglycan binding of CCL5 and CCL3." Proc Natl Acad Sci U S A **113**(18):
544 5000-5005.
545 Lim, H. W., P. Hillsamer, A. H. Banham and C. H. Kim (2005). "Cutting edge: direct
546 suppression of B cells by CD4+ CD25+ regulatory T cells." J Immunol **175**(7): 4180-
547 4183.
548 Linterman, M. A., W. Pierson, S. K. Lee, A. Kallies, S. Kawamoto, T. F. Rayner, M.
549 Srivastava, D. P. Divekar, L. Beaton, J. J. Hogan, S. Fagarasan, A. Liston, K. G. Smith
550 and C. G. Vinuesa (2011). "Foxp3+ follicular regulatory T cells control the germinal
551 center response." Nat Med **17**(8): 975-982.
552 Maurer, M. and E. von Stebut (2004). "Macrophage inflammatory protein-1." Int J
553 Biochem Cell Biol **36**(10): 1882-1886.
554 Menten, P., A. Wuyts and J. Van Damme (2002). "Macrophage inflammatory protein-1."
555 Cytokine Growth Factor Rev **13**(6): 455-481.
556 Patterson, S. J., A. M. Pesenacker, A. Y. Wang, J. Gillies, M. Mojibian, K. Morishita, R.
557 Tan, T. J. Kieffer, C. B. Verchere, C. Panagiotopoulos and M. K. Levings (2016). "T
558 regulatory cell chemokine production mediates pathogenic T cell attraction and
559 suppression." J Clin Invest **126**(3): 1039-1051.
560 Qi, H., J. L. Cannons, F. Klauschen, P. L. Schwartzberg and R. N. Germain (2008).
561 "SAP-controlled T-B cell interactions underlie germinal centre formation." Nature
562 **455**(7214): 764-769.
563 Sage, P. T., L. M. Francisco, C. V. Carman and A. H. Sharpe (2013). "The receptor PD-1
564 controls follicular regulatory T cells in the lymph nodes and blood." Nat Immunol **14**(2):
565 152-161.
566 Sage, P. T., A. M. Paterson, S. B. Lovitch and A. H. Sharpe (2014). "The coinhibitory
567 receptor CTLA-4 controls B cell responses by modulating T follicular helper, T follicular
568 regulatory, and T regulatory cells." Immunity **41**(6): 1026-1039.
569 Sage, P. T., N. Ron-Harel, V. R. Juneja, D. R. Sen, S. Maleri, W. Sungnak, V. K.
570 Kuchroo, W. N. Haining, N. Chevrier, M. Haigis and A. H. Sharpe (2016). "Suppression
571 by TFR cells leads to durable and selective inhibition of B cell effector function." Nat
572 Immunol **17**(12): 1436-1446.
573 Shulman, Z., A. D. Gitlin, J. S. Weinstein, B. Lainez, E. Esplugues, R. A. Flavell, J. E.
574 Craft and M. C. Nussenzweig (2014). "Dynamic signaling by T follicular helper cells
575 during germinal center B cell selection." Science **345**(6200): 1058-1062.
576 Victora, G. D., D. Dominguez-Sola, A. B. Holmes, S. Deroubaix, R. Dalla-Favera and M.
577 C. Nussenzweig (2012). "Identification of human germinal center light and dark zone
578 cells and their relationship to human B-cell lymphomas." Blood **120**(11): 2240-2248.
579 Wing, J. B., W. Ise, T. Kurosaki and S. Sakaguchi (2014). "Regulatory T cells control
580 antigen-specific expansion of Tfh cell number and humoral immune responses via the
581 coreceptor CTLA-4." Immunity **41**(6): 1013-1025.
582 Wing, J. B. and S. Sakaguchi (2014). "Foxp3(+) T(reg) cells in humoral immunity." Int
583 Immunol **26**(2): 61-69.
584 Wollenberg, I., A. Agua-Doce, A. Hernandez, C. Almeida, V. G. Oliveira, J. Faro and L.
585 Graca (2011). "Regulation of the germinal center reaction by Foxp3+ follicular regulatory
586 T cells." J Immunol **187**(9): 4553-4560.
587 Wu, H., Y. Chen, H. Liu, L. L. Xu, P. Teuscher, S. Wang, S. Lu and A. L. Dent (2016).
588 "Follicular regulatory T cells repress cytokine production by follicular helper T cells and
589 optimize IgG responses in mice." Eur J Immunol **46**(5): 1152-1161.

590
591
592
593
594
595
596
597
598
599
600
601
602
603
604
605
606
607
608
609
610
611 **FIGURES**
612

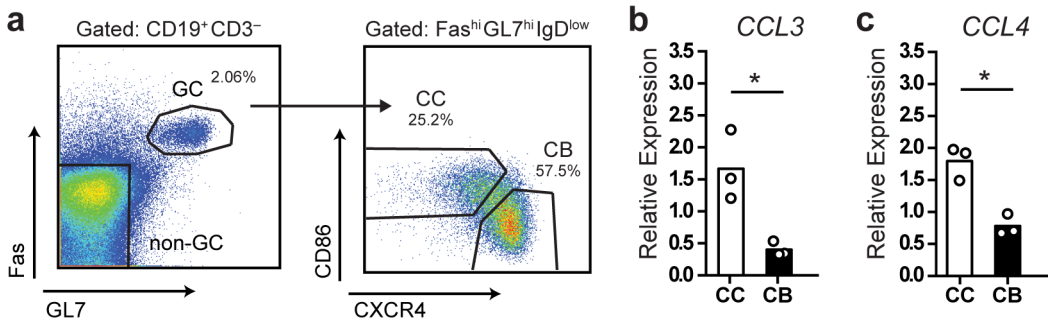


613
614

615 **Figure 1. A small subset of GC centrocytes upregulates CCL3/4 expression**. qRT-PCR
616 analysis of CCL3 and CCL4 expression in GC and non-GC B cells sorted from the draining LNs of
617 mice s.c. immunized with 50 $\mu$g ovalbumin (OVA) in Ribi at 10 days post immunization (d.p.i). **a**,

The gating strategy for cell sorting. **b, c**, Relative expression of CCL3/4 in bulk GC centroblasts (CB) and centrocytes (CC) as normalized to non-GC B cells ($FAS^{low}$ $GL7^{low}$). Chemokine $C_T$ values were normalized to β2m $C_T$. Bars represent mean with dots representing average values per experiment. Data represent n=3 independent experiments, 4 mice total. *, $P<0.05$, two-tailed Student's *t*-test.

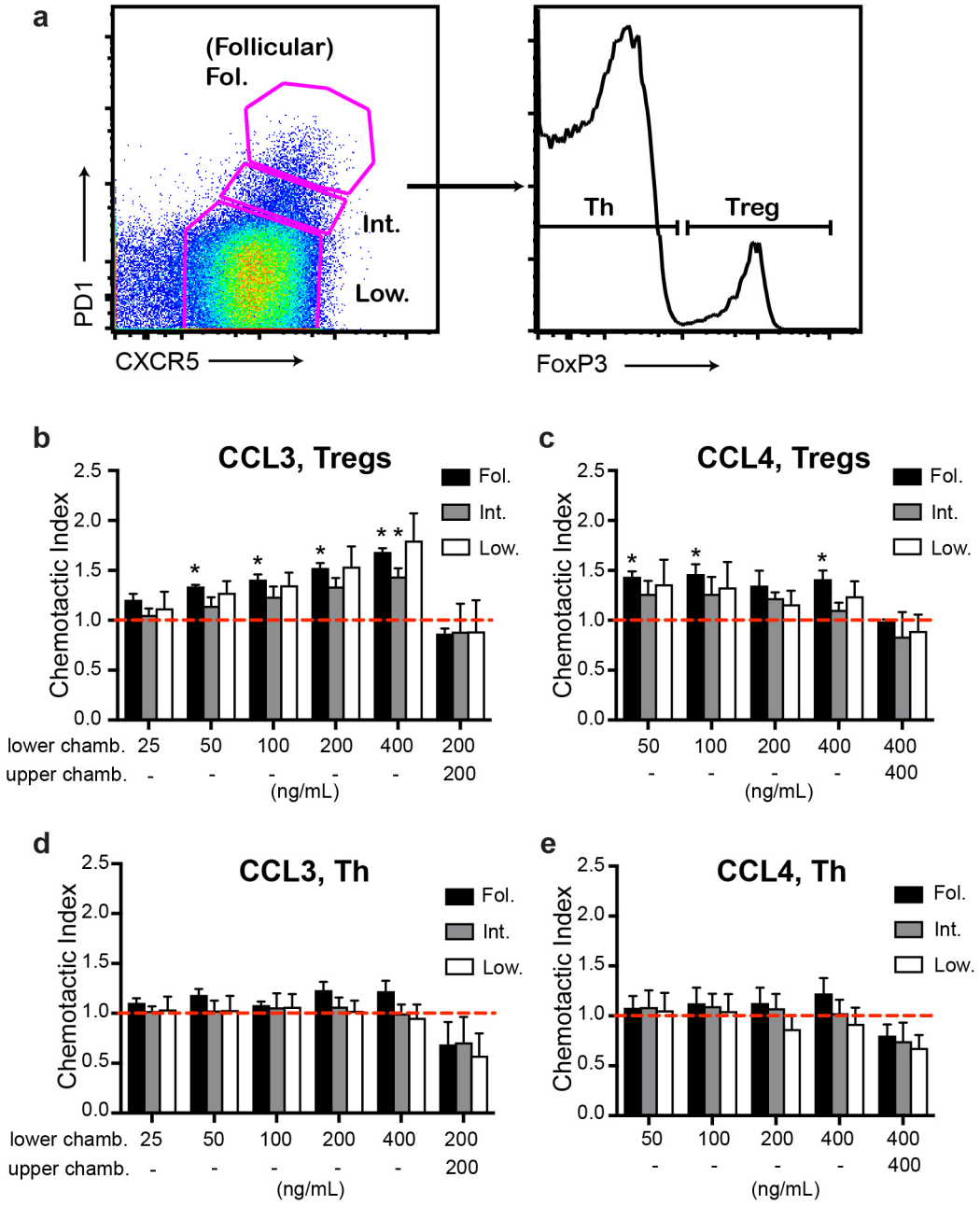


**Figure 2**. **Chemotaxis of Tfr cells to CCL3 and CCL4 *ex vivo*. a-e,** *Ex vivo* transwell assay of $CD4^+$ T cells purified from dLNs of WT mice at 10 d.p.i. with 100 $\mu$g OVA in Ribi and analyzed by flow cytometry using the gating strategy as in (a). Transmigration of $CXCR5^{high}PD1^{high}$ (Fol., black bars), $CXCR5^{int}PD^{int}$ (Int., grey bars), or $CXCR5^{low}PD1^{low}$ (Low, white bars) $CD4^{pos}$ $CD8^{neg}$ B220 $^{neg}$ cell populations that also express Foxp3 (b, c) or were FoxP3 $^{neg}$ (d, e) were measured against CCL3 (b, d) and CCL4 (c, e). The chemokines were added either to the lower chambers (chamb.) of transwells for analysis of chemotaxis or to both the upper and the lower chambers for analysis of chemokinesis. Chemotactic index was calculated as the ratio of cells that transmigrated towards the chemokine vs. no chemokine control (dashed red line). Chemotaxis and chemokinesis data are derived from 3 and 2 independent experiments correspondingly with 2 mice per experiment. Bars represent mean ± SEM, *, P<0.05, two-tailed, one-sample Student's *t*-test (compared to 1).

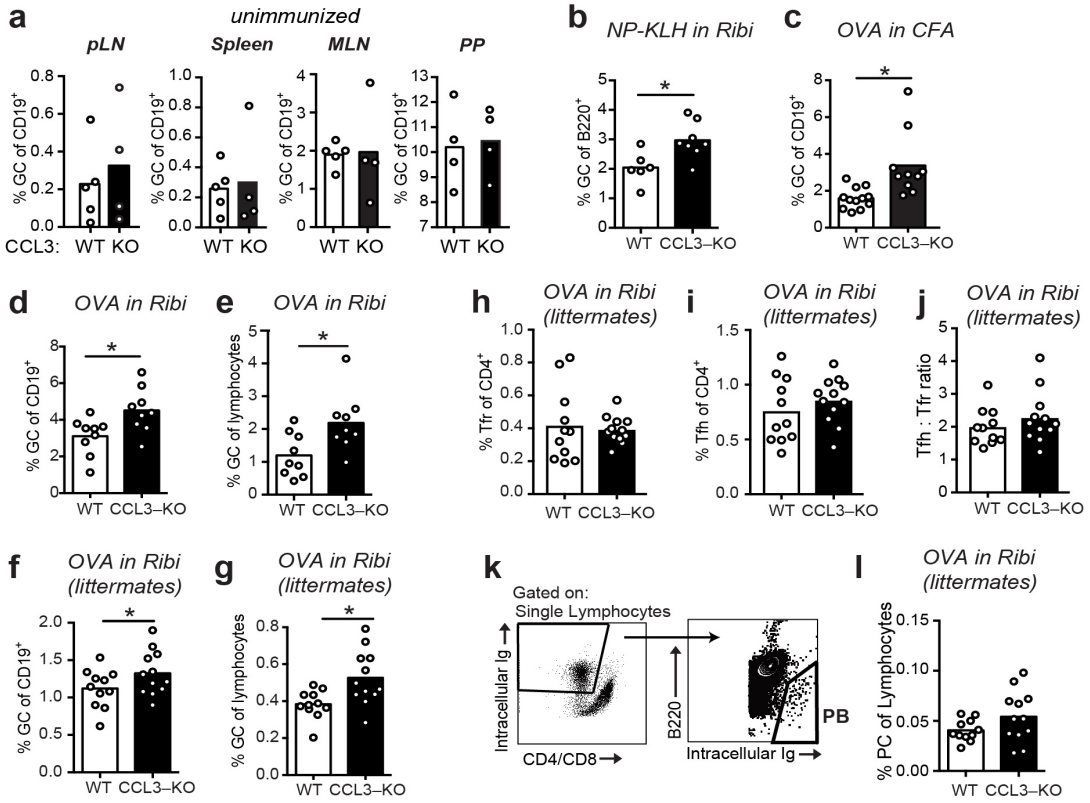


**Figure 3. Increased GC response in CCL3-KO mice following immunization**. **a-g**, Flow cytometry analysis of the GC B cells (Fas$^{high}$ GL7$^{high}$ IgD$^{low}$) as a fraction of total B cells (a-d, f) or total lymphocytes (e, g) in WT and CCL3-KO mice. **a**, Analysis of GCs in pLNs (inguinal, brachial and auxillary LNs combined), spleens, MLNs, and PP from unimmunized mice. **b-g**, Analysis of GCs in the dLNs from mice s.c. immunized with 50 $\mu$g of 4-Hydroxy-3-nitrophenyl (*NP*) acetyl-*hapten* conjugated to *Keyhole limpet hemocyanin (*KLH) in Ribi adjuvant (b) or 50 $\mu$g of OVA in Complete Fruend's Adjuvant (CFA) (c) or 50 $\mu$g OVA in Ribi (d-g) at 10 d.p.i. **f-l,** Flow cytometry analysis of GC (f, g), Follicular T cell (h-j), and plasma cell (PC) (k, l) response in dLNs of WT and CCL3-KO littermate conrol mice s.c. immunized with 50 $\mu$g OVA in Ribi at 10 d.p.i. **h-j**, Tfr (CXCR5$^{high}$ PD1$^{high}$ FoxP3$^{pos}$ in h) and Tfh (CXCR5$^{high}$ PD1$^{high}$ FoxP3$^{neg}$ in i) cells as a fraction of CD4 T cells. **k, l**, PB gating strategy (k) and PBs as a fraction of total lymphocytes (l). Each symbol represents one mouse. Bars represent mean. Data are derived from 2 or 3 independent experiments. *, P<0.05, Student's *t*-test (two-sided in b-e, one-sided in f, g).

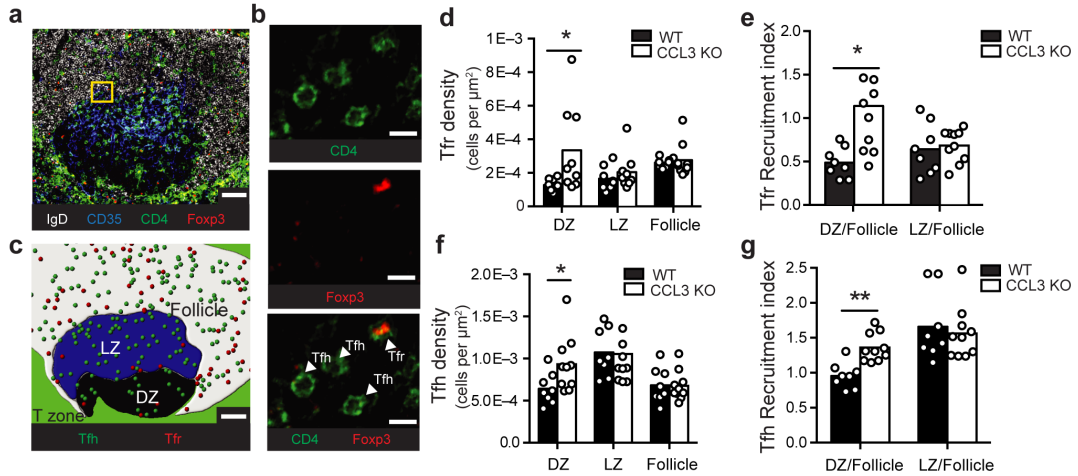


**Figure 4. CCL3 does not recruit Tfr or Tfh cells into the GC light zone.** Immunofluorescent analysis of Tfr and Tfh cell localization in the GCs and follicles of draining pLNs from WT or CCL3-KO mice at 10 d.p.i. with 50 µg OVA in Ribi. **a-c**, Representative example of a confocal image of pLN section and its analysis. **a**, Confocal image of a GC-containing 10 µm section of pLN from WT mouse, stained with antibodies against IgD (white), CD35 (blue), CD4 (green) and Foxp3 (red). **b**, Magnified image from the inset (in **a**) that illustrates how Treg ($CD4^+Foxp3^+$) and Th ($CD4^+Foxp3^-$) cells were identified. **c**, Reconstruction of GC light zone (blue area), dark zone (black area), follicle (white area), Tregs (red circles) and Th cells (green circles) within the confocal image shown in (**a**) using manually defined surfaces in Imaris. Scale bars – 50 µm in **a**, **c** and 10 µm in **b**. **d-g** Quantitative analysis of Treg (**d, e**) and Th (**f, g**) cell abundance in the GCs and the follicles. Density of Tregs (**d**) and Th cells (**f**) in GC dark zone (DZ), light zone (LZ) and follicles around GCs calculated as the number of T cells in each zone normalized to the total area of that zone. Recruitment index calculated as the density of Tregs (**e**) or Th cells (**g**) in GC DZ or LZ normalized to their density in the GC-containing follicle. **d-g**, Each symbol represents analysis of pLN section with a distinct GC. Data represents n=3 independent experiments with 4 total mice per genotype. Bars represent mean. *, P<0.05, two-tailed Student's *t*-test.

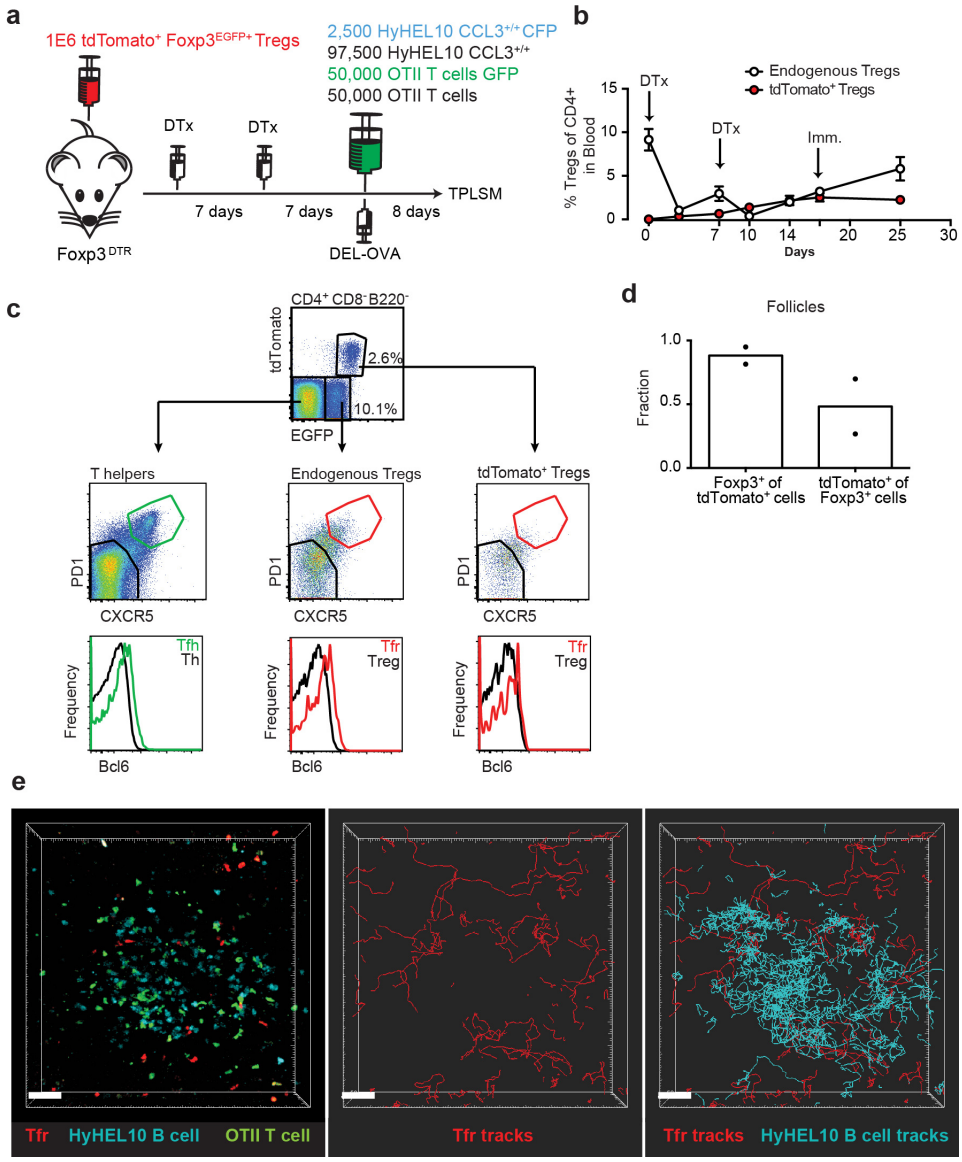


**Figure 5. 2P visualization of Tfr cells and HyHEL10 GC B cells. a**, Experimental diagram for generation of recipient mice with large numbers of highly fluorescent tdTomato$^{+}$ Tregs and visualization of Tfr and HyHEL10 (Hy10) GC B cells in the dLNs by 2P microscopy. **b**, Flow cytometry analysis of the endogenous and transferred TdTomato$^{+}$ Treg numbers in the blood of FoxP3$^{DTR}$ mice throughout their treatments with DTx and immunization, performed as in (a). **c-e**, Analysis of dLNs from mice generated through the procedure described in (a) at 8 d.p.i. **c**, Representative flow cytometry analysis of Bcl6 expression in the CXCR5$^{low}$PD1$^{low}$ and CXCR5$^{high}$PD1$^{high}$ subsets of tdTomato$^{+}$ Tregs (top panels), endogenous Tregs (middle panels) and endogenous Th cells (bottom panels). **d**, Confocal immunofluorescence analysis of dLN sections for the fraction of tdTomato$^{+}$ cells that express Foxp3 (left bars) and fraction of Foxp3+ cells that express tdTomato$^{+}$ (right bars) in GC-containing follicles.**e**, Representative 2P imaging analysis of Tfr cells localization with respect to GCs. A snapshot (left panel) from an intravital imaging experiment as analyzed in Imaris software. Cell trajectory analysis for Tfr cells (middle panel) and both Tfr cells and GC B cells (right panel). Scale bars 40 µm. Data are from 2 independent experiments.

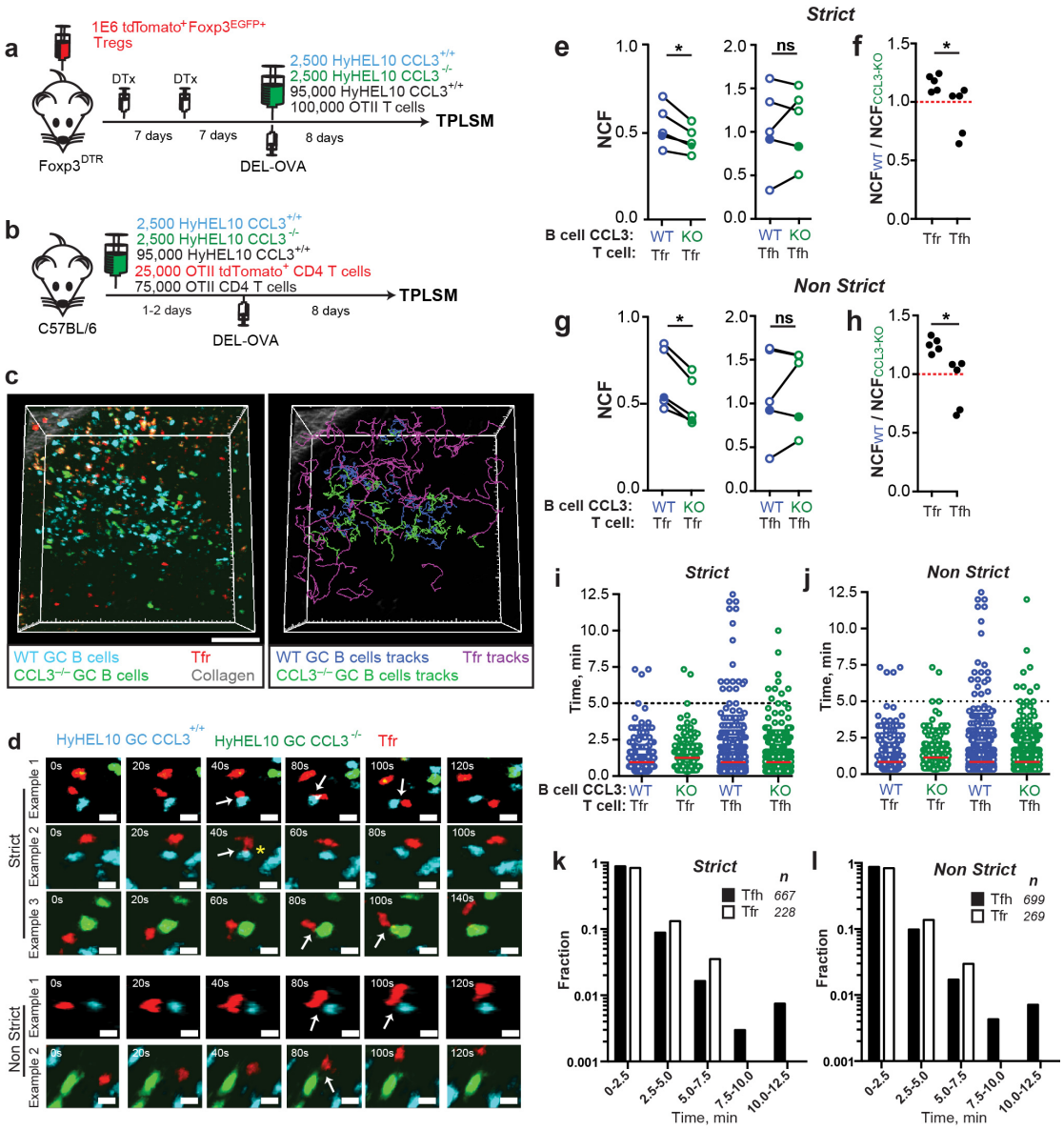


**Figure 6. Tfr cells make less frequent contacts with CCL3-KO B cells in GCs.** 2P imaging analysis of Tfr and Tfh cells contacts with CCL3$^{+/+}$ CFP and CCL3$^{-/-}$ GFP HyHEL10 GC B cells in the dLNs of mice at 8 d.p.i. **a, b**, Experimental diagrams for imaging GC B cell interactions with Tfr (a) and Tfh (b). **c**, A snapshot (**left panel**) and cell trajectory analysis (**right panel**) from an intravital imaging experiment performed as described in a**.** Scale bars - 50 μm. Auto-fluorescent cells are orange. **d,** Time-lapse images of Tfr cells interacting with CCL3$^{+/+}$ or CCL3$^{-/-}$ HyHEL10 B cells within GCs. Cell contacts were verified in 3D space, classified as Strict (definitive contacts) and Non Strict (all possible contacts) and indicated by white arrows. Yellow star illustrates pseudopod extension by a Tfr cell towards CFP GC B cell. Images are displayed as 20 $\mu$m z-stacks. Scale bars - 5 μm. **e-j**, Quantitative analysis of CCL3$^{+/+}$ (blue circles) and CCL3$^{-/-}$ (green circles) HyHEL10 GC B cell interactions with Tfr or Tfh cells. Closed symbols represent intravital and opened symbols - explanted dLNs imaging. The data was analyzed in a blinded fashion to avoid possible bias in cell contact definition. **e, g,** Normalized contact frequency (NCF) calculated for Strict (e) and Non Strict (g) as the number of Tfr or Tfh cells' interactions with CCL3$^{+/+}$ and CCL3$^{-/-}$ HyHEL10 B cells within defined volume of GCs normalized to the average number of HyHEL10 cells of each genotype. Linked symbols correspond to GC B

764 cells in the same movie. *, P<0.05, Wilcoxon matched-pairs test. **f, h,** Ratios of the Tfr or Tfh cell
765 NCF with $CCL3^{+/+}$ over $CCL3^{-/-}$ HyHEL10 B cells from the same movie. *, P<0.05, Student's t-
766 test. **i, j**, Contact duration between Tfr or Tfh and HyHEL10 GC B cells of each genotype
767 undergoing Strict (i) or Non Strict (j) interactions. Red lines represent medians. Data from 5
768 independent experiments (5 mice) per T cell type. **k, l,** Time histograms for duration of strict (k)
769 and non-strict (l) contacts between Tfr and Tfh cells with WT HyHEL10 GC B cells.
770
771
772
773
774
775
776
777
778
779
780
781
782
783
784
785
786
787
788
789
790
791
792
793
794
795
796
797
798
799
800
801
802
803
804
805
806
807
808
809
810
811
812
813
814
815
816

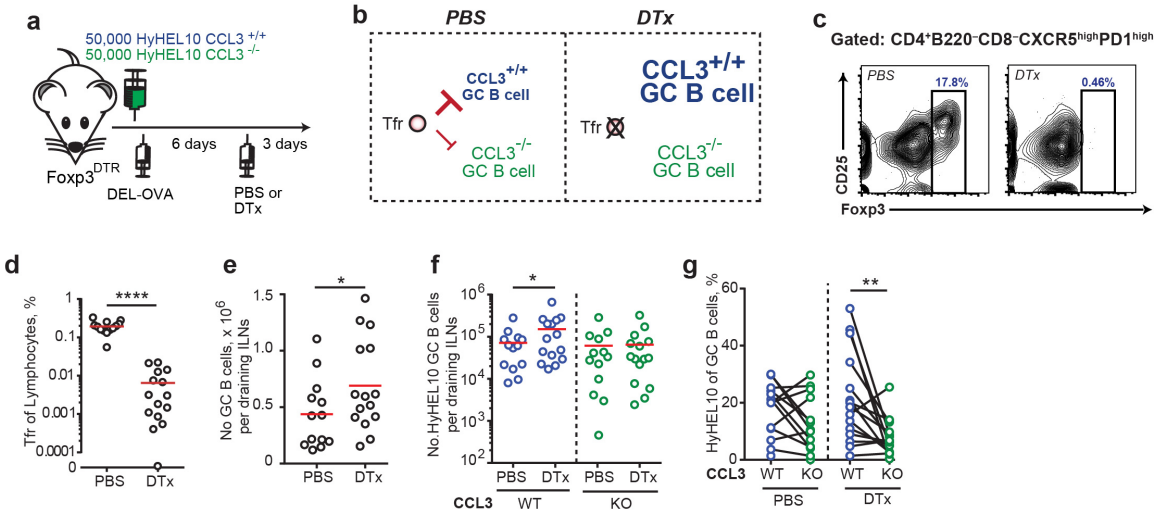


**Figure 7. Tregs repress B cell participation in GCs at 9 d.p.i. in a CCL3-dependent way. a**, Experimental outline. FoxP3$^{DTR}$ recipient mice were transferred with HyHEL10 B cells, immunized with 50 µg DEL-OVA in Ribi s.c. and then treated either with PBS or 5 µg DTx in PBS i.p. 3 days before analysis. **b**, Suggested model of CCL3-dependent regulation of GC B cells by Tfr cells and prediction for CCL3$^{+/+}$ and CCL3$^{-/-}$ GC B cell participation in GCs upon ablation of Tfr cells at 9 d.p.i. **c-g**, Flow cytometry analysis of cell participation in immune response at 9 d.p.i. in DTx-treated and control mice. **c-e,** DTx-mediated depletion of Tfr cells at 9 d.p.i. Representative example of Tfr ablation (in c) and Tfr fraction of total lymphocytes (in d) and increase in GC response in DTx-treated mice (in e). **f, g,** CCL3$^{+/+}$ and CCL3$^{-/-}$ HyHEL10 GC B cells in PBS and DTx-treated mice shown as the total numbers of cells in dLNs (f) or as the % of total GC B cells. The data are from 5 independent experiments. Each dot represents a single mouse and red lines correspond to the mean values. Paired analyses are indicated using solid black line. *, $p<0.05$, **, $p<0.01$, ****, $P<0.0001$. Two-sided (in d, g) or one-sided (in e, f) Student's t-test.

855 **SUPPLEMENTARY FIGURES**

856

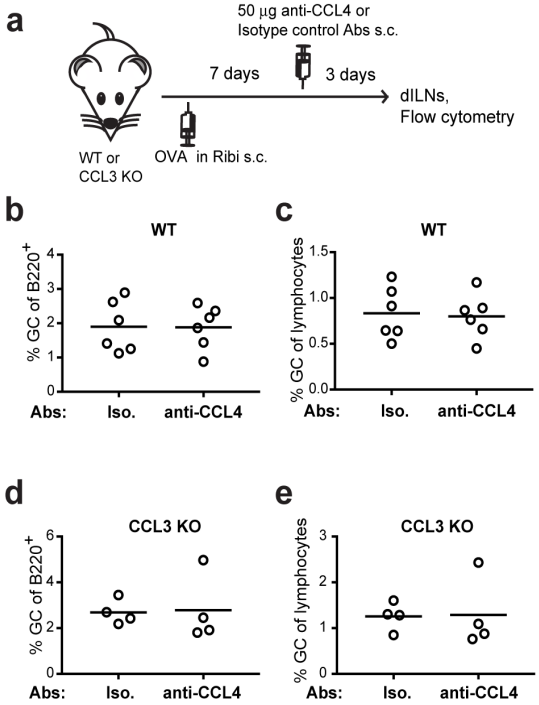


**Supplementary Figure 1. CCL4 neutralization in GCs does not amplify GC response in WT or CCL3-KO mice. a**, Experimental strategy. **b-e**, GC B cells ($B220^{pos}$ $CD4^{neg}$ $CD8^{neg}$ $FAS^{high}$ $GL7^{high}$) in the dLNs of WT (b, c) and CCL3-KO (d, e) mice as a fraction of $B220^{+}$ cells (b, d) or lymphocytes (c, d) at 10 d.p.i. with OVA in Ribi.

857
858
859
860
861

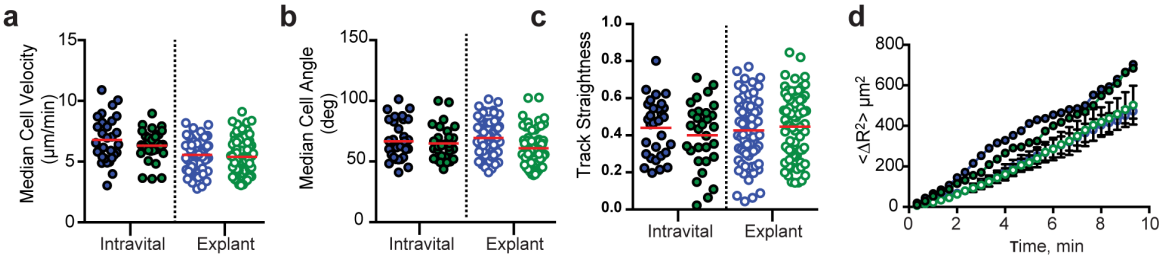


**Supplementary Figure 2: HyHEL10 GC $CCL3^{+/+}$ CFP (blue circles) and $CCL3^{-/-}$ GFP (green circles) cell motility analysis. Red lines represent medians. Data are from 4 independent experiments.**

862
863
864
865
866
867
868
869

870 **SUPPLEMENTARY MOVIE LEGENDS**
871
872 **Movie S1. 2-photon imaging of Tfr cells migration in respect to Tfh cells and GC B**
873 **cells.** Also see **Figure 5e**. A time-lapse sequence of a 110 µm z-stack of a GC in an
874 explanted inguinal lymph node imaged at 8 days after immunization. HyHEL10 GC B
875 cell; cyan. Tfr; red. Tfh; green. Colored lines indicate the trajectories of the indicated cell
876 types, tracked by Imaris and manually verified. Mice were generated as described in the
877 **Figure 5a**. Time is shown as hh:mm:ss and z-stacks were acquired at 20 second
878 intervals.

879 **Movie S2. Intravital imaging of Tfr cells in respect to the GCs containing both**
880 **$CCL3^{+/+}$ and $CCL3^{-/-}$ HyHEL10 B cells.** The data shown corresponds with the images in
881 **Figure 6**. A time-lapse sequence of a GC within inguinal LN of a mouse prepared as
882 described in **Figure 6a** and subjected to intravital imaging at 8 days post immunization.
883 180 µm z-stack. GC volume (gray surface) was defined based on the distribution of CFP
884 HyHEL10 cells. Quantitative analysis in **Figure 6e-l** was performed for Tfr cells (red)
885 interactions with HyHEL10 GC B cells ($CCL3^{+/+}$; cyan. $CCL3^{-/-}$; green.) within GC
886 volumes defined in the same fashion. The tracks of individual Tfr cells outside the GC
887 are labeled in purple while interior tracks are represented in yellow lines. Time is
888 expressed as hh:mm:ss and z-stacks were acquired at 20 second intervals.

889 **Movie S3. Examples of Tfr cells interactions with GC B cells identified as "strict"**
890 **or "nonstrict" for quantitative analysis.** A time-lapse sequence of a representative Tfr
891 (red) entering the GC (dashed white line) and then undergoing contacts with HyHEL10
892 $CCL3^{+/+}$ (cyan) or $CCL3^{-/-}$ (green) HyHEL10 GC B cells within inguinal LN of a mouse
893 prepared as described in **Figure 6a** and subjected to 2P imaging at 8 days post
894 immunization. A 40 $\mu$M slice is in view. Inlets are zoomed in and 3D rotated to visualize
895 the contact. Time is expressed as mm:ss and z-stacks were acquired at 25 second
896 intervals

897 **Movie S4. 2-photon imaging of Tfh cells interacting with GC B cells**. A time-lapse
898 sequence of a GC within an inguinal LN of a mouse prepared as described in **Figure 6b**
899 and subjected to explant imaging at 8 days post immunization. 140 um z-stack**.**
900 Quantitative analysis was performed for Tfh cells (red) interactions with HyHEL10 GC B
901 cells ($CCL3^{+/+}$, cyan; $CCL3^{-/-}$, green) within the GC and can be found in **Figure 6e-l**.
902 Examples of long duration (>5 minutes) contacts and short duration (<5 minutes)
903 contacts are shown in 10 um z-projections. Time is shown as hh:mm:ss for both time of
904 the movie and for duration of the indicated contacts. Z-stacks were acquired at 20
905 second intervals.

906
907
908
909